 doi:10.20944/preprints202209.0184.v1

Article

On the Use of a Non-Constant Non-Affine or Slip Parameter in Polymer Rheology Constitutive Modeling

Vasileios-Martin Nikiforidis,[1] Dimitrios G Tsalikis,[2] and Pavlos S. Stephanou[1]

[1]Department of Chemical Engineering, Cyprus University of Technology, PO Box 50329, 3603 Limassol, Cyprus
[2]Department of Chemical Engineering, University of Patras & FORTH/ICE-HT, Patras, GR 26504, Greece
* Correspondence: Tel.: +357-25-002394, fax: +357-25-002668, e-mail: pavlos.stefanou@cut.ac.cy

Abstract: Since its introduction, back in the late 1970s, the non-affine or slip parameter, ξ, has been routinely employed by numerous constitutive models as a constant parameter. However, the evidence seems to imply that it should be a function of polymer deformation. In the present work, we phenomenologically modify a constitutive model for the rheology of unentangled polymer melts [P. S. Stephanou et al. J. Rheol. 53, 309 (2009)] to account for a non-constant slip parameter. The revised model predictions are compared against newly accumulated rheological data for a C_{48} polyethylene melt obtained via direct non-equilibrium molecular dynamics simulations in shear. We find that the conformation tensor data are very well predicted; however, the predictions of the material functions are noted to deviate from the NEMD data, especially at large shear rates.

Keywords: unentangled systems; constitutive modeling; materials functions; non-affine parameter; slip parameter; conformation tensor; NEMD simulations; atomistic simulations; polyethylene

1. Introduction

Fundamental understanding of the rheological and microstructural behavior of polymeric fluids under flow is essential in practical polymer processing operations. Polymers are fluids that exhibit a non-Newtonian rheological character that stems from their internal microstructure. The dynamical behavior of the microstructure is usually challenging to obtain experimentally, leaving ample space for computational simulations. Nowadays, due to the growth of computational power and the advent of sophisticated computational algorithms, experiments executed computationally offer the only alternative to experiments that cannot be conducted physically [1]. This is particularly true for polymeric materials, even the simplest of all, i.e., linear polyethylene (PE) chains, since one must span a spectrum of orders of magnitude in both time and space [1]. Today, simulations, particularly atomistic ones (i.e., simulations in which individual atoms of ensembles of molecules are tracked in phase space) offer the best avenue to validate theories without hypotheses, such as the Rouse theory for cyclic polymers (rings) [2] or the tube notion in entangled polymeric systems (i.e., systems whose molecular weights exceeds the entanglement molecular weight, and whose dynamics is dictated by a slithering or snake-like motion within a confining mean-field tube produced by the surrounding chain molecules) [3]. However, a similar success has not been accomplished yet in non-equilibrium systems, i.e., systems away from equilibrium, such as those under flow, is more complicated to simulate [1].

Still, non-equilibrium molecular dynamics simulations (NEMD) simulations have provided invaluable insight into the dynamical behavior of polymer chains under flow. Experimentally, although it has been possible to directly visualize individual polymer chains when subjected to flow, such as the work of Smith et al. [4] and LeDuc et al. [5], who used video microscopy to study the dynamics of individual, tagged chains under shear in dilute solutions of DNA and noted that these chains exhibit both deformation and

Preprints (www.preprints.org) | NOT PEER-REVIEWED | Posted: 14 September 2022 doi:10.20944/preprints202209.0184.v1

tumbling motions, these experiments can only track a small number of molecules at any given time. This void has been filled recently by atomistic NEMD simulations since every single chain can accurately be tracked. Indeed, the rotation or tumbling of polymer chains has been noted through the execution of NEMD simulations to occur for both unentangled and entangled chains if the flow field possesses a rotational contribution, such as simple shear flow [6–15]. Recent research has unambiguously clarified that the tumbling of polymer chains leads to the appearance of a transient stress undershoot (following the overshoot) at high shear rates [16,17]. It remains, however, as to how this tumbling behavior can be considered in constitutive modeling.

Since its introduction, back in the late 1970s by Gordon and Schowalter (GS) [18] and Johnson and Segalman (JS) [19], the non-affine or slip parameter, ξ, has been routinely employed by numerous constitutive models. This parameter allows for the "slippage" of polymer chains relative to the surrounding medium (either solvent in polymer solutions or surrounding polymer chains in polymer melts) [20]. This slippage, allows for a rotation of the polymer chain when subjected to shear. When ξ=0, the chain deforms affinely, and thus no rotation is allowed, whereas when $\xi = 1$ the chain is completely rigid, as they are not allowed to deform [20]. Note that in general, ξ is considered to be $0 \le \xi \le 2$: when $\xi = 0$, the mixed derivative found in the GS-JS model reduces to the upper-convected Maxwell derivative, when $\xi = 1$ to the corotational derivative, whereas when $\xi = 2$ to the lower-convected Maxwell derivative. However, as pointed out by Öttinger [21], the inverse of a lower-convected tensor is of an upper-convected type, explaining why the thermodynamic admissibility condition, i.e., the second law of thermodynamics, limits the range of ξ to only the first subdomain $0 \le \xi \le 1$ [22]. This can further be justified by noting that the choice $\xi = 0$ describes the affine motion of either a flexible polymer chain or infinite aspect ratio solid ellipsoid, whereas as the aspect ratio decreases, the choice $\xi = 1$ describes the limit of spherical solid particles with the elastic contribution to the stress decreasing to zero [23].

The slip parameter has long been considered a given constant, despite numerous indications that it should increase as the flow field intensifies. Since the rotational contribution in shear intensifies as the shear rate increases, this rotational or dumping behavior of polymer chains also intensifies, meaning that the slip parameter should also increase. Furthermore, since close to equilibrium the field is not strong enough to force chain tumbling (thereby not resulting in the exhibition of an undershoot in the transient shear viscosity at small shear rates), we should expect the slip parameter to vanish. Also, since this slip is typically observed with rigid particles due to flow-induced torque, slip can be considered a measure of molecular rigidity [20]. This is a strong function of the particle's aspect ratio, as can be deduced from the fact that the evolution equation for the trace-constrained orientation tensor of rigid ellipsoid includes a mixed-convected derivative similar to the GS derivative with $\xi = (p^2 - 1)/(p^2 + 1)$ where p is the particle's aspect ratio [20,24].

Possibly the first to consider a variable slip parameter were Hinch [25] and Rallison and Hinch [26]. They considered a modification of the finite-extensible non-linear elastic (FENE) dumbbell model by considering a slip parameter given via, using our nomenclature, $\xi = \mathrm{tr}\mathbf{C}/\left(\frac{1}{3}\langle R^2\rangle_{\mathrm{eq}}\beta + \mathrm{tr}\mathbf{C}\right)$ where $\mathbf{C}$ is the dimensional conformation tensor, and $\langle R^2\rangle_{eq}$ is the average squared end-to-end polymer distance at equilibrium (see also next Section) [26]. However, as the polymer aspect ratio decreases due to deformation, one would expect that ξ should also be time-dependent. Such a consideration has not been considered in the past, with the sole exception being the work of Beris et al.[27] who introduced a phenomenological kinetic equation for the slip parameter. They also introduced a limiting value for the non-affine parameter at high shear rates. However, in their model, the slip parameter was only coupled to the shear rate and not the structure itself. To the best of our knowledge, there has not been any other work wherein a (shear rate or time) dependent slip parameter was considered.

Although other constitutive models have considered a variety of mechanisms to accommodate the tumbling of polymer chains under shear, such as the use of a "tumbling"

Preprints (www.preprints.org) | NOT PEER-REVIEWED | Posted: 14 September 2022 doi:10.20944/preprints202209.0184.v1

function by Costanzo et al. [17] or the explicit consideration of rotational diffusion by Stephanou et al. [28–30], the necessity to have a variable slip parameter remains. In this work, we will generalize the constitutive model for unentangled polymer melts of Stephanou et al. [22] to accommodate a variable slip parameter by including an additional evolution equation for ξ, following our recent work on the use of a scalar structural variable [31–33].

The paper is structured as follows: in Sec. 2 the new model is introduced, whereas Sec. 3 presents the details concerning the simulated system and technical information regarding the MD and NEMD simulations performed. Then, in Sec. 4 we present the model predictions along with a comparison with the simulation data accumulated. The paper concludes with Sec. 5, where we elaborate on the significance of our work and discuss future plans.

2. Model modification

Following previous work [22,23], we define the conformation tensor as the second moment of the distribution function $\Psi(\mathbf{R},\mathbf{r},t)$ for the chain end-to-end vector **R,** with its center-of-mass at position **r**, i.e., $C_{\alpha\beta}(\mathbf{r},t)=\langle R_\alpha R_\beta\rangle(\mathbf{r},t)=\int R_\alpha R_\beta \Psi(\mathbf{R},\mathbf{r},t)d\mathbf{R}$ with the brackets denoting a configurational average. The evolution equations for the dimensionless conformation tensor $c_{\alpha\beta}(\mathbf{r},t)=3C_{\alpha\beta}(\mathbf{r},t)/\langle R^2\rangle_{eq}$, as derived by Stephanou et al. [22], is

$$\dot{c}_{\alpha\beta,[JS]}=-\frac{B(\mathbf{c})}{\tau_R(\mathrm{tr}\mathbf{c})}\big[\delta_{\alpha\gamma}+\alpha(1-\xi)B(\mathbf{c})\big(h_0(\mathrm{tr}\mathbf{c})c_{\alpha\gamma}-\delta_{\alpha\gamma}\big)\big]\big(h_0(\mathrm{tr}\mathbf{c})c_{\gamma\beta}-\delta_{\gamma\beta}\big), \tag{1a}$$

where

$$\dot{c}_{\alpha\beta,[JS]}=\dot{c}_{\alpha\beta,[1]}+\frac{\xi}{2}\big(c_{\alpha\gamma}\dot{\gamma}_{\beta\gamma}+c_{\beta\gamma}\dot{\gamma}_{\gamma\alpha}\big), \tag{1b}$$

denotes the GS or JS mixed derivative, with $\dot{\boldsymbol{\gamma}}\equiv\nabla\mathbf{u}+(\nabla\mathbf{u})^T$ being the rate-of-deformation tensor ($\mathbf{X}^T$ is the transpose of $\mathbf{X}$). Also, α is the anisotropic Giesekus parameter,

$$h_0(\mathrm{tr}\mathbf{c})=\frac{b-3}{b-\mathrm{tr}\mathbf{c}}, \tag{1c}$$

is the effective spring "constant", accounting for finite extensible non-linear (FENE) effects with b the FENE parameter, and the function

$$B(\mathbf{c})=\left(\frac{b}{b+a_0(\mathbf{c})}\right)^2, \tag{1d}$$

with $0\le B(\mathbf{c})\le 1$, ensures that the entropy density remains bounded even at high deformation rates [34] with $a_0(\mathbf{c})$ the dimensionless unbounded free energy [22,35] given as

$$a_0(\mathbf{c})=\Phi(\mathrm{tr}\mathbf{c})-\ln\det\mathbf{c}, \tag{1e}$$

$$\Phi(\mathrm{tr}\mathbf{c})=-(b-3)\ln\left(1-\frac{\mathrm{tr}\mathbf{c}-3}{b}\right), \tag{1f}$$

and the relaxation, or Rouse, time

$$\tau_R(\mathrm{tr}\mathbf{c})=\tau_{R,\mathrm{eq}}\exp[-\varepsilon(1-\xi)B(\mathbf{c})(h_0(\mathrm{tr}\mathbf{c})\mathrm{tr}\mathbf{c}-3)], \tag{1g}$$

with ε the Phan-Thien Tanner parameter, and $\tau_{R,\mathrm{eq}}$ is the equilibrium Rouse time. Note that other expressions could also be employed, such as the Extended White-Metzner

Preprints (www.preprints.org) | NOT PEER-REVIEWED | Posted: 14 September 2022 doi:10.20944/preprints202209.0184.v1

expression [23,31,36]. Finally, the corresponding expression relating the stress tensor with the conformation tensor is given as,

$$\sigma_{\alpha\beta} = G(1-\xi)B(\mathbf{c})\left(h_0(\mathrm{tr}\mathbf{c})c_{\alpha\beta} - \delta_{\alpha\beta}\right), \quad (2)$$

where G is the elastic modulus.

We now proceed to modify the Stephanou et al. [22] model by considering a variable slip parameter. To this end, we simply propose here an expression for the evolution equation of ξ bearing in mind our previous work concerning the scalar structural variable λ [31–33]:

$$\frac{D\xi}{Dt} = -\frac{\xi}{\tau_\xi} + (\xi_0 - \xi)\boldsymbol{\kappa}:\mathbf{c}, \quad (3)$$

where $\boldsymbol{\kappa} = (\nabla\mathbf{u})^T$, τ_ξ is the characteristic time for the increase of the slip parameter, and ξ_0 is the limiting value of the slip parameter at large shear rates. The first term in Eq. (3) is a relaxation term returning the slip parameter back to its equilibrium, null, value when the flow is stopped, whereas the second is a term that increases the slip parameter as a result of the applied flow.

2.1. Asymptotic Behavior of the Model for steady-state and transient Shear flow

Here, we analyze the asymptotic behavior of the revised model in the limits of low and high shear rates for both steady-state and transient simple shear flow described by the kinematics $\mathbf{u} = (\dot{\gamma}y, 0, 0)$, where $\dot{\gamma}$ is the shear rate (x is the flow direction, y the velocity gradient direction, and z the neutral direction). The material functions to analyze are the shear viscosity $\eta \equiv \sigma_{yx}/\dot{\gamma}$ and the two normal stress coefficients $\Psi_1 \equiv (\sigma_{xx} - \sigma_{yy})/\dot{\gamma}^2$ and $\Psi_2 \equiv (\sigma_{yy} - \sigma_{zz})/\dot{\gamma}^2$, respectively. By expanding the conformation tensor and the slip parameter up to second order terms in the dimensionless shear rate, $\mathrm{Wi} = \dot{\gamma}\tau_{R,\mathrm{eq}}$, we arrive at the following expressions for the conformation tensor and the slip parameter

$$c_{xx} = 1 - (\alpha - 2)\mathrm{Wi}^2, \quad (4a)$$

$$c_{xy} = \mathrm{Wi} \quad (4b)$$

$$c_{yy} = 1 - \alpha\mathrm{Wi}^2 \quad (4c)$$

$$c_{zz} = 1 \quad (4d)$$

$$\xi = \xi_0\gamma\mathrm{Wi}^2 \quad (4e)$$

and for the zero-shear-rate shear viscosity and normal stress coefficients,

$$\eta_0 = G\tau_{R,\mathrm{eq}}, \quad (5a)$$

$$\Psi_{1,0} = 2\eta_0\tau_{R,\mathrm{eq}}, \quad (5b)$$

$$-\Psi_{2,0} = \frac{\alpha}{2}\Psi_{1,0}, \quad (5c)$$

There are the same as the ones presented by Stephanou et al. [22] by considering $\xi = 0$ in their Eqs. (41) and (42). On the other hand, at large shear rates the slip parameter will approach the value ξ_0, see next Section.

Preprints (www.preprints.org) | NOT PEER-REVIEWED | Posted: 14 September 2022 doi:10.20944/preprints202209.0184.v1

Upon inception of simple shear flow, the explicit solutions for the time-dependent viscometric functions in the linear viscoealastic limit, following the methodology of Stephanou et al. [35], are given as

$$\eta^+(t) = \eta_0 \left[1 - \exp\left(-\frac{t}{\tau_{R,\mathrm{eq}}}\right)\right], \tag{6a}$$

$$\Psi_1^+(t) = \Psi_{1,0} \left[1 - \left(1 + \frac{t}{\tau_{R,\mathrm{eq}}}\right)\exp\left(-\frac{t}{\tau_{R,\mathrm{eq}}}\right)\right], \tag{6b}$$

$$\Psi_2^+(t) = \Psi_{2,0} \left[1 - \frac{2t}{\tau_{R,\mathrm{eq}}}\exp\left(-\frac{t}{\tau_{R,\mathrm{eq}}}\right) - \exp\left(-\frac{2t}{\tau_{R,\mathrm{eq}}}\right)\right], \tag{6c}$$

3. Molecular Model and System Studied

In this work, we conducted equilibrium molecular dynamics (MD) simulations, and NEMD simulations of polyethylene (PE) oligomer $C_{48}H_{98}$ melts. Equilibrium MD simulations were performed in the NPT ensemble to fully relax the initial PE configurations at temperature T = 450 K and P = 1 atm using the united-atom potential model of Siepmann et al. [37]. The simulations were carried out using the LAMMPS simulation engine [38], employing the Nosé-Hoover thermostat [39] and the Parrinello-Rahman barostat [40] to preserve the temperature and pressure, respectively, at their prescribed values. Subsequently, several fully relaxed configurations from the MD runs were selected as input for the NEMD simulations under shear. The NEMD runs were performed again with LAMMPS in the NVT ensemble at T = 450 K, using the SLLOD algorithm, [41] together with the Nosé-Hoover thermostat to control the temperature. The microscopic set of equations of motion was integrated numerically using the reversible Reference System Propagator Algorithm (r-RESPA) [42], with 2 different time steps: (a) a large one (dt = 4 fs) for the integration of the slowest varying forces arising from non-bonded interactions at long interatomic distances, and (b) a small one (dt = 0.5 fs) for the integration of the fast-varying forces corresponding to the bonded (i.e., bonds, angles, and dihedrals) interactions.

All simulations were conducted using large cells containing 16000 chain molecules of $C_{48}H_{98}$ and were subject to periodic boundary conditions in all three directions (x, y, and z). In the course of the NEMD simulations, the x- and y- directions were selected as the flow and the shear gradient directions, respectively, whereas z was the so-called neutral direction. The simulation cell had dimensions (462 Å) × (231 Å) × (231 Å) along the x, y, and z directions. The cell was purposefully enlarged in the (x-) flow direction so as to ensure minimal system size effects, particularly with the NEMD runs at high shear rates where the polymer chains tend to stretch and orient towards the flow direction. To this end, for the $C_{48}H_{98}$ chains, the equilibrium root-mean-square of the chain end-to-end vector $\langle R^2\rangle_{\mathrm{eq}}$ and the theoretical maximum chain extension of $|R|_{\max}$ were calculated and came out to be equal to $\langle R^2\rangle_{\mathrm{eq}} = 27.2 \pm 0.12$ Å and $|R|_{\max} = 63.1$ Å, respectively. Compared to the simulation cell dimensions, the maximum chain length $|R|_{\max}$ is 7.3 times shorter than the dimension in the x-direction and 3.6 times shorter than the dimension in the y-direction. Thus, we can safely expect that the simulation cell is sufficiently large to ensure the absence of system size effects due to chain alignment in the flow direction or tumbling motion in the shear gradient direction.

In the course of the equilibrium MD simulations, the equilibrium orientational relaxation time $\tau_{R,\mathrm{eq}}$ of the simulated $C_{48}H_{98}$ PE chains at T = 450 K and P = 1 atm was found to be equal to $\tau_{R,\mathrm{eq}} = 0.6 \pm 0.01$ ns, as estimated by integrating over time the stretched-exponential curve [43] describing the time autocorrelation function of the chain end-to-

Preprints (www.preprints.org) | NOT PEER-REVIEWED | Posted: 14 September 2022 doi:10.20944/preprints202209.0184.v1

end unit vector. The MD simulations were conducted for a total of 6 ns, which is 10 times larger than the chain relaxation time to ensure that the PE chains are fully equilibrated. The NEMD simulations were executed over a broad range of shear rates spanning the range from the linear up to the highly nonlinear viscoelastic regime, corresponding to Weissenberg numbers (with $\tau_{R,\mathrm{eq}} = 0.6$ ns) in the interval [0.1, 285].

4. Results and discussion

4.1. Model predictions in steady-state shear flow

In this section, we present the predictions of the new model in the case of steady-state shear flow. The results have been obtained by numerically solving the constitutive model, Eqs. (1), using Matlab [44] and then calculating the stress tensor, Eq. (2). In the following, we define $\gamma = \tau_{\xi}/\tau_{R,\mathrm{eq}}$.

In Fig. 1, we depict the model prediction for the slip parameter as a function of Wi and its

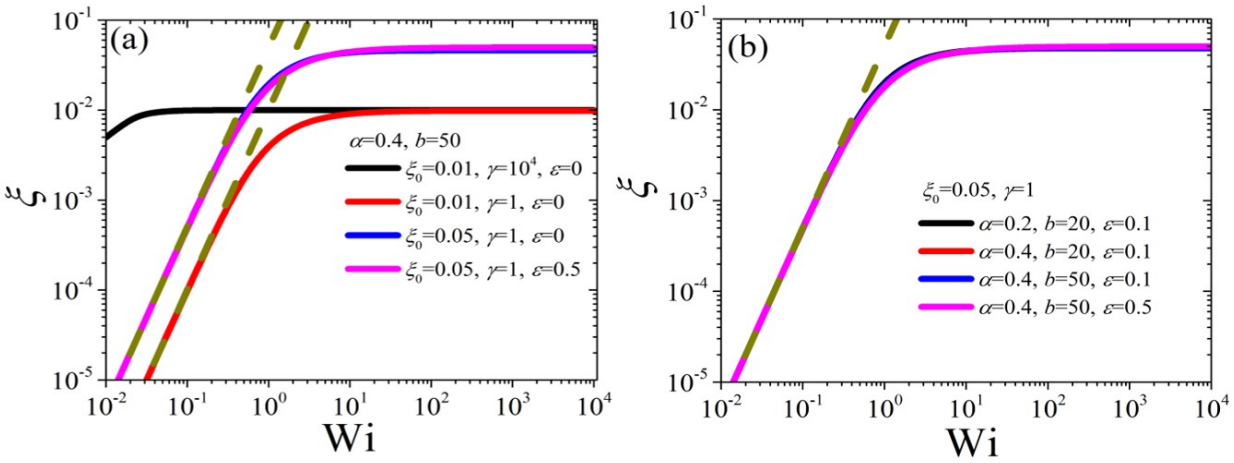

Figure 1: Model predictions for the slip parameter as a function of Wi and dependence on: (a) the parameters ξ_0, γ and ε for $\alpha = 0.4, b = 50$, and (b) the parameters $\alpha, \varepsilon,$ and b for of $\xi_0 = 0.05$ and $\gamma = 1$.

Preprints (www.preprints.org) | NOT PEER-REVIEWED | Posted: 14 September 2022 doi:10.20944/preprints202209.0184.v1

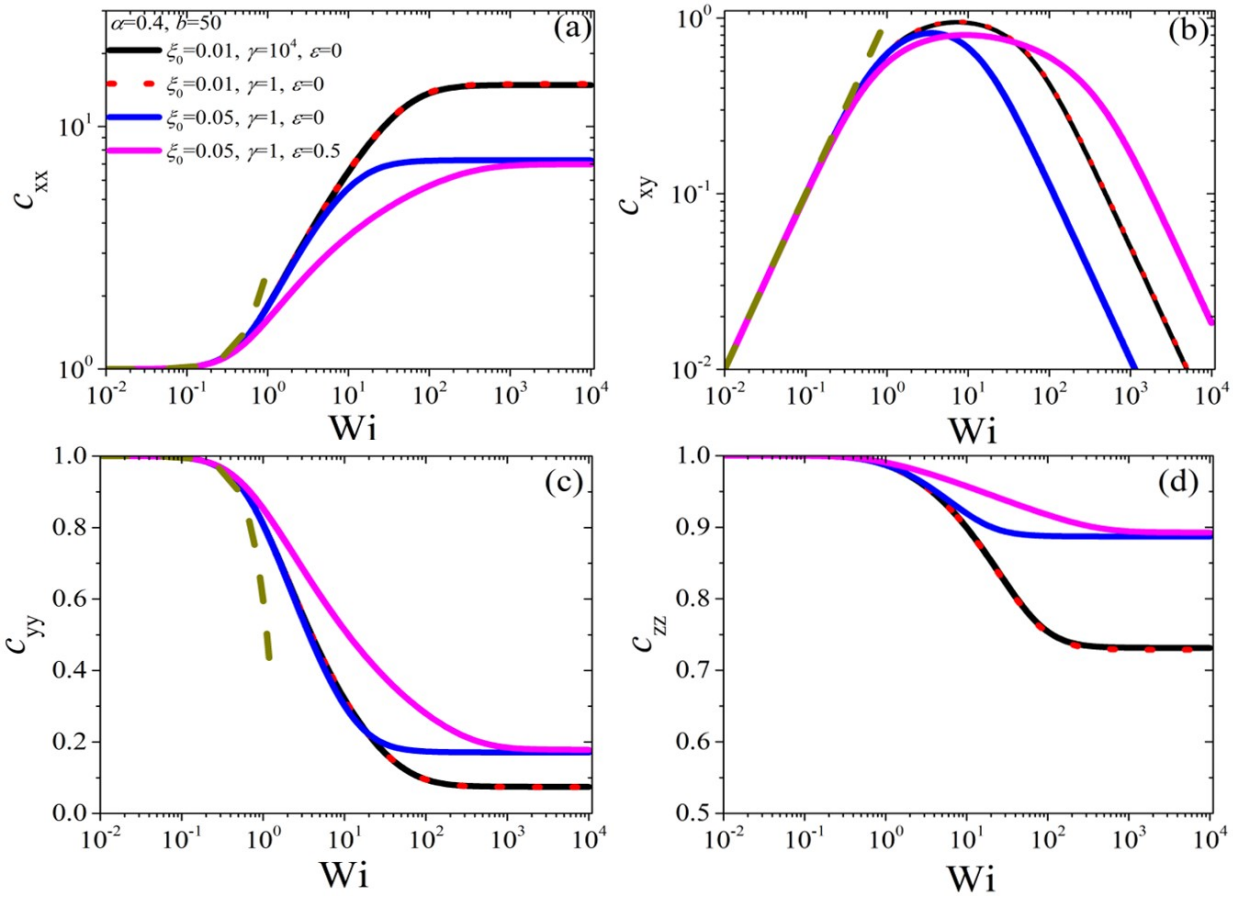

Figure 2: Variation of the conformation tensor with Wi and dependence on the parameters ξ_0, γ and ε for $\alpha = 0.4, b = 50$. The dark yellow dashed line depicts the asymptotic behavior at small shear rates given by Eqs. (4).

dependence on the parameters ξ_0, γ and ε while keeping constant $\alpha = 0.4, b = 50$ [panel (a)], and

(b) the parameters $\alpha, \varepsilon,$ and b while keeping constant $\xi_0 = 0.05, \gamma = 1$ [panel (b)]. As noted in Fig. 1(a), at large values of γ the slip parameter steeply reaches its limiting value, which is unaltered as the shear rate increases further. This situation resembles the previous version of the model [22] where the slip parameter was considered a constant. However, as γ is reduced to unity, the slip parameter increases with the shear rate and reaches its limiting value at about Wi=10. As the

Preprints (www.preprints.org) | NOT PEER-REVIEWED | Posted: 14 September 2022 doi:10.20944/preprints202209.0184.v1

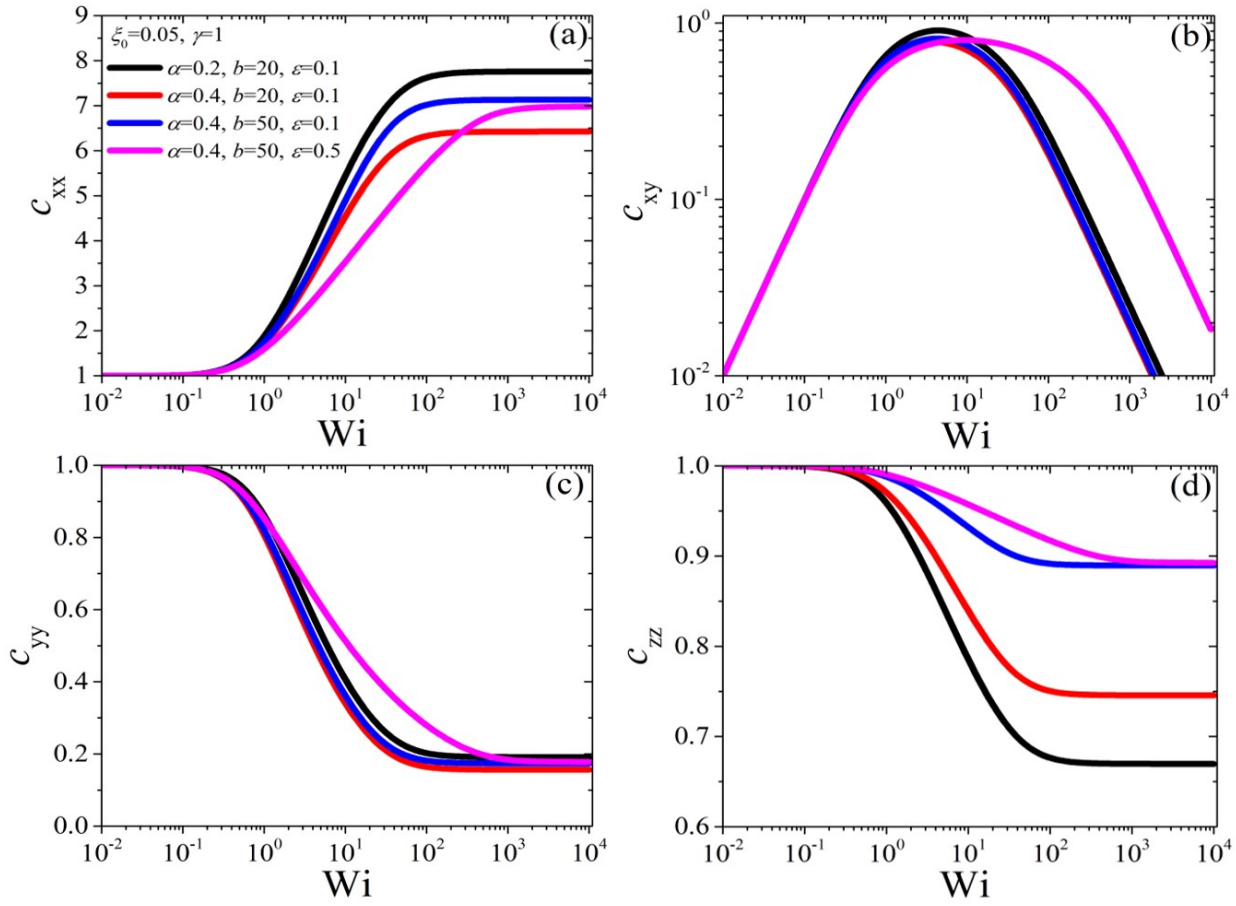

Figure 3: Same as Fig. 2 but for the parameters $\alpha, \varepsilon,$ and b for $\xi_0 = 0.05$ and $\gamma = 1$.

parameter ξ_0 increases, the curve seems to shift upwards, whereas by increasing ε we note a slight shift upwards at larger shear rates. This is because when $\varepsilon = 0$ the slip parameter does not fully reach its limiting value since c_{xy} delays its reduction with the shear rate, as shown in Fig. 2(b). On the other hand, the slip parameter seems to be insensitive to the precise values of α and b [panel (b)]. Note that in all cases, the analytical expression Eq. (4e) is accurate until about Wi=1.

Next, in Fig. 2, we depict the model predictions of the conformation tensor as a function of Wi whilst keeping $\alpha = 0.4, b = 50$ constant, whereas in Fig. 3, we depict the same comparison whilst keeping $\xi_0 = 0.05, \gamma = 1$. Irrespective of the values of the parameters (see both Figs. 2 and 3), we note that c_{xx} is reported to increase from its equilibrium value after about Wi=0.1 and eventually reaching its limiting value, which however differs from the value of the parameter b. On the other hand, c_{xy} is noted to increase linearly with the shear rate, reaches a maximum value, and then starts decreasing inversely proportional to the shear rate. Finally, the two remaining diagonal elements in the shear gradient direction and neutral direction conformation tensor, respectively, (c_{yy} and c_{zz}, respectively) are observed to be mirrors of the noted behavior of c_{xx}: they initially decrease from their equilibrium value, eventually reaching a finite asymptotic value at high shear rates. We note, in Fig. 2, that the value of γ plays only a very modest role for all components, since the value of the slip parameter is small; do note that one would expect such small values to be used since larger values would lead to very intense oscillations in the time-dependent material functions (results not shown). On the other hand, by increasing the parameter ξ_0, we note the predictions at low shear rates to be insensitive, but the limiting asymptotic values at high shear rates are noted to decrease for c_{xx} and increase for both c_{yy} and c_{zz}, whereas the c_{xy} curve shifts to lower shear rates at higher shear rates whilst keeping the

Preprints (www.preprints.org) | NOT PEER-REVIEWED | Posted: 14 September 2022 doi:10.20944/preprints202209.0184.v1

power-law unaffected. This is a direct result of allowing tumbling to occur sooner, since the slip parameter is more significant, thus refraining the flow to deform the chain further. Finally, when we increase the value of ε while keeping the same ξ_0 and γ values, we note that the asymptotic values of the diagonal components remain the same, but the curves are shifted to the right, a direct result of the steeper decrease of the relaxation time, cf. Eq. (1g). As the anisotropic (or Giesekus) parameter is increased, we note the curve of c_{xx} to shift downwards and the one of c_{zz} to shift upwards (see Fig. 3), whereas when the FENE parameter is increased (from 20 to 50, meaning that the chain now is longer or its molecular weight is larger) we note the reverse behavior, which is the expected outcome. However, note that during these parameter value changes, the predictions of the other

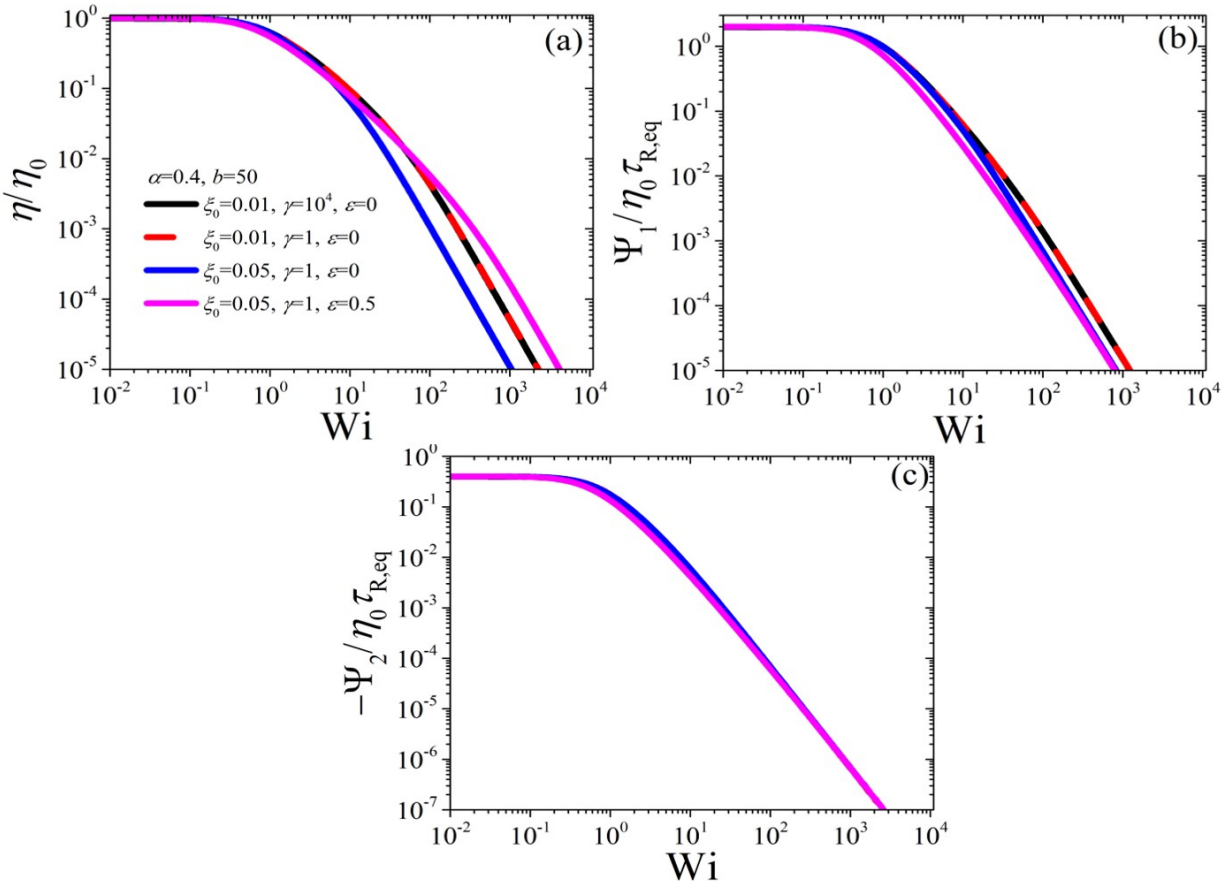

Figure 4: Variation of the materials functions as a function of Wi and dependence on the parameters ξ_0, γ and ε for $\alpha = 0.4, b = 50$.

two components, c_{xy} [panel (b)] and c_{yy} [panel (c)] are only modestly affected. As in Fig. 2, the value of ε controls the rate at which the asymptotic values, in the case of the diagonal elements, are reached, whereas the c_{xy} curve shifts to rightwards.

In Fig. 4 and Fig. 5 we depict the same comparison as Figs. 2 and 3, respectively, but for the three dimensionless materials functions: the shear viscosity, η,[panel (a)], and the first, Ψ_1, [panel (b)] and negative second, $-\Psi_2$, [panel (c)] normal stress coefficients. We again note, in Fig. 4, that the predictions are insensitive to the value of the slip parameter due to the small value of ξ_0. By increasing the value of ξ_0, both η and Ψ_1 are noted to shift to smaller shear rates, which

Preprints (www.preprints.org) | NOT PEER-REVIEWED | Posted: 14 September 2022 doi:10.20944/preprints202209.0184.v1

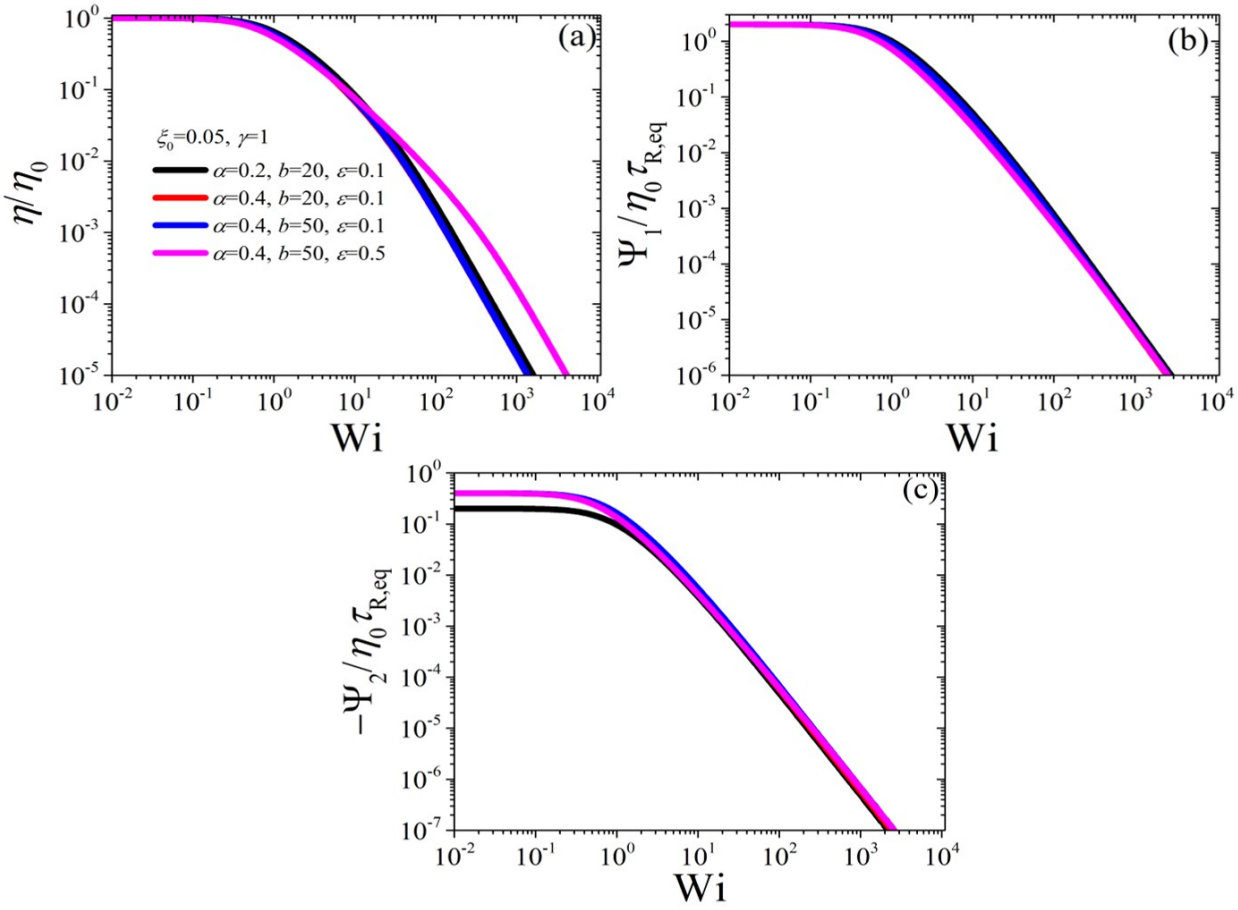

Figure 5: Same as Fig. 4 but for the parameters α, ε and b for of $\xi_0 = 0.05$ and $\gamma = 1$.

is much more intense in the former case, whereas when increasing ε, we note the shear viscosity curve to shift to larger shear rates, and Ψ_1 to remain almost unaltered at large shear rates, but shifts rightwards at intermediate Wi. On the contrary, $-\Psi_2$ is noted to be almost completely unaffected. Finally, Fig. 5 shows that for both η and Ψ_1 are invariant to changes in the values of α and b. On the other hand, the zero-shear-rate second normal stress coefficient increases as the Giesekus parameter increases, cf. Eq. (5c), but again remains invariant at higher shear rates.

4.2. Comparison with NEMD simulation data for an unentangled PE melt

In this section, we aim to compare the predictions of the revised model against rheological data obtained through newly-accumulated, fully atomistic, NEMD simulations of a short unentangled C_{48} PE melt over a wide spectrum of shear rates. We will only analyze the steady-state data of these NEMD simulations. To fit the simulation data, following Stephanou et al. [22], we first identify the asymptotes c_{ii}^{∞} of the diagonal elements of the conformation tensor in the limit of high shear rates. Also, the equilibrium relaxation (Rouse) time, as mentioned in Sec. 3, is equal to $\tau_{R,\mathrm{eq}} = 0.6$ ns, whereas the zero-shear-rate viscosity can be obtained from the shear viscosity NEMD data, equal to $\eta_0 = 5$ mPa. s. Please note that as small shear rates the NEMD data of the viscometric functions come with large error bars, and it is difficult, particularly for the normal stress coefficients,

Preprints (www.preprints.org) | NOT PEER-REVIEWED | Posted: 14 September 2022 doi:10.20944/preprints202209.0184.v1

to estimate their zero-shear-rate values. Then, the value of $\xi_0 \approx 0.104$ is obtained by using the first equation of Eqs. (45) of Stephanou et al. [22]. Next, the value of the Giesekus parameter $\alpha \approx 0.2$ can be obtained by fitting the Ψ_2 NEMD data at low shear rates and using Eq. (4c) [the value of $\Psi_{1,0}$ is easily calculated from eq. (4b)]. Note that this value differs from the value $\alpha \approx 0.06$ obtained by using the second equation of Eqs. (45) of Stephanou et al. [22]; however, the fitting of Ψ_2 is much improved when using the former value, and the comparison against the conformation tensor data is only mildly worsened. Next, the value of b=5.78 can be obtained from Eq. (48) of Stephanou et al. [22]. The remaining two parameters, ε and γ, can be obtained by simply fitting the NEMD data, since they do not affect the c_{ii}^{∞} values; we obtain $\varepsilon = 0.4$ and $\gamma = 0.01$. Figure 6 shows how well the new model can fit the simulation data for the c_{xx}, c_{xy}, c_{yy}, and c_{zz} components of the dimensionless conformation tensor for the C_{48}

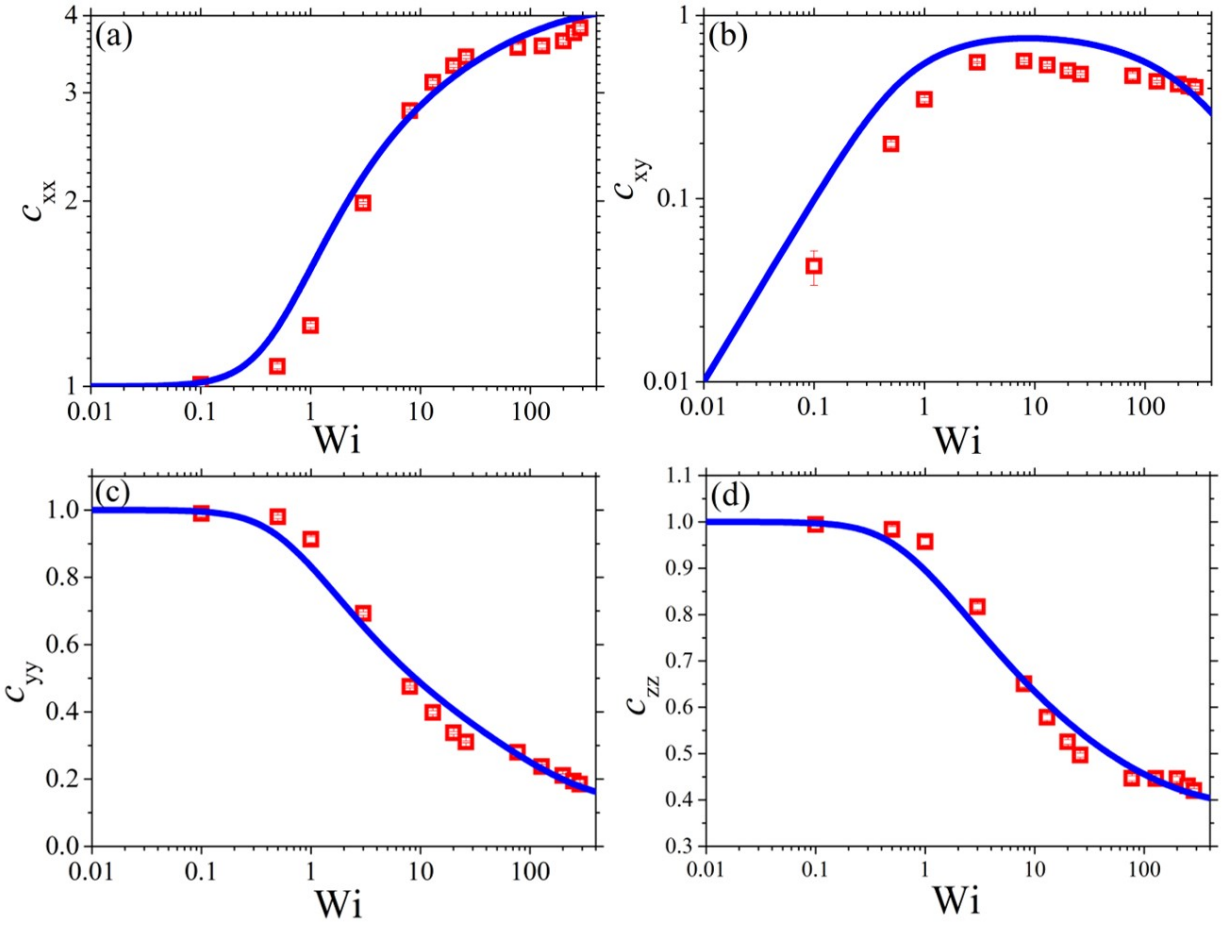

Figure 6: Model predictions (blue line) for the nonzero components of the conformation tensor c in steady shear for the C_{48} PE melt along with comparison with the NEMD simulation results (red squares).

PE system in steady shear. We note that the predictions of the revised model are in a remarkable agreement with the NEMD extracted simulation results over the entire wide range of shear rates considered, especially for the diagonal elements. The corresponding comparison for the material functions η, Ψ_1, and $-\Psi_2$ is presented in Fig. 7. Contrary to the almost excellent agreement between the refined model predictions and the NEMD simulation data for the dimensionless conformation tensor, the comparison against the viscometric functions is less satisfactory. Deviations from the NEMD data are mainly observed at large shear rates in the case of the shear

Preprints (www.preprints.org) | NOT PEER-REVIEWED | Posted: 14 September 2022 doi:10.20944/preprints202209.0184.v1

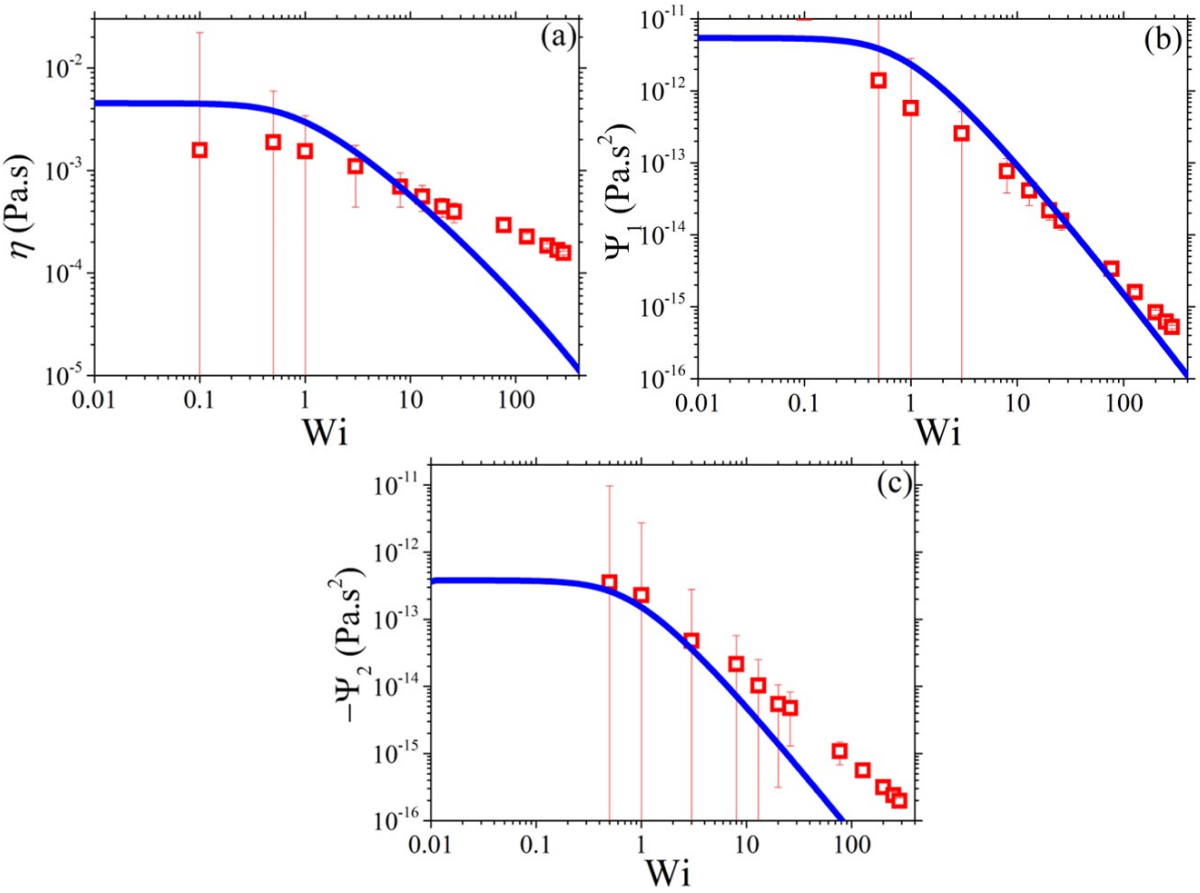

Figure 7. Same as with Figure 6 but for the material functions.

viscosity [panel (a)] and the second normal stress coefficient [panel (c)], as also mentioned by Stephanou et al. [22], should be related to the postulated relation between stress and conformation tensors, Eq. (2), which stems from the assumption of purely entropic elasticity [45]. As such, we need to invoke a more accurate expression for the free energy in the future [22].

5. Conclusions

It is today well established, both experimentally [4,5] and computationally [6–15], that polymer chains subjected to flow fields that possess a rotational contribution exhibit, in addition to deformation, a tumbling/rotational behavior, which is unambiguously responsible for the appearance of a transient stress undershoot (following the overshoot) at high shear rates [16,17,35]. This rotational behavior has been related to the "slippage" of polymer chains, relative to its surrounding, which in constitutive models is considered, among other methodologies, via the non-affine or slip parameter, ξ [18–20,22,35]. Although this parameter has been exclusively considered to be a constant, evidence suggests it should be a function of the chain's aspect ratio [20]. Probably, with the sole exception of the works of Rallison and Hinch [25,26] and Beris et al. [27], no other constitutive model has considered a shear-rate- (and time-) dependent slip parameter.

In our present work, we have modified a constitutive model [22] that has been quite successful in predicting the data, both on the level of the conformation tensor but also the

viscometric functions, obtained from detailed atomistic NEMD simulations of unentangled polymer systems over a wide molecular weight span, to accommodate a variable slip parameter. The central idea is that the increase of the slip parameter from its equilibrium (null) value should be both shear-rate- and time-dependent due to the increasing rotational contribution of the imposed shear flow as the shear rate increases. The revised model still accounts for the most significant effects realized in physical systems, such as anisotropic drag, finite extensibility, non-affine motion, variable chain relaxation, and a bounded non-equilibrium free energy, all together as introduced in its predecessor [22]. We have compared the predictions of the revised model against newly executed atomistic NEMD simulations of a short unentangled PE melt with a molecular length equal to C_{48}. Although the predictions at large shear rates have not been modified significantly, the revision has amended the problems associated with having ξ-dependent zero-shear-rate viscometric functions [22,35], cf. Eqs. (4), and linear-viscoelastic properties [35] , cf. Eqs. (5). It should be emphasized that although the revised model has not been derived through the use of a non-equilibrium thermodynamics formalism [21,23], its thermodynamic admissibility still holds, since $0 \leq \xi \leq 1$ always holds (provided $0 \leq \xi_0 \leq 1$). Also, it is a straightforward exercise to extend the model to entangled systems by following our recent work [35]. We expect that the future use of the refined model will allow for the more reliable prediction of macroscopic viscoelastic behavior and, therefore, for the development of more reliable computational tools aiming to tailor-design large-molecular-weight polymeric systems.

Author Contributions: Conceptualization, Pavlos Stephanou; Data curation, Vasileios-Martin Nikiforidis; Formal analysis, Vasileios-Martin Nikiforidis; Funding acquisition, Pavlos Stephanou; Investigation, Vasileios-Martin Nikiforidis; Methodology, Pavlos Stephanou; Project administration, Pavlos Stephanou; Resources, Vasileios-Martin Nikiforidis and Dimitrios Tsalikis; Software, Vasileios-Martin Nikiforidis, Dimitrios Tsalikis and Pavlos Stephanou; Supervision, Dimitrios Tsalikis and Pavlos Stephanou; Validation, Vasileios-Martin Nikiforidis and Dimitrios Tsalikis; Visualization, Vasileios-Martin Nikiforidis; Writing – original draft, Vasileios-Martin Nikiforidis; Writing – review & editing, Dimitrios Tsalikis and Pavlos Stephanou.

Funding: This work was funded by the Cyprus University of Technology through the Starting grant of P.S.S. (Project Acronym.: NET-CST).

Institutional Review Board Statement: Not applicable

Informed Consent Statement: Not applicable

Data Availability Statement: Not applicable

Conflicts of Interest: The author declares no conflict of interest.

References

1. Edwards, B.J.; Nafar Sefiddashti, M.H.; Khomami, B. Atomistic Simulation of Shear Flow of Linear Alkane and Polyethylene Liquids: A 50-Year Retrospective. *J. Rheol.* **2022**, *66*, 415, doi:10.1122/8.0000365.
2. Tsolou, G.; Stratikis, N.; Baig, C.; Stephanou, P.S.; Mavrantzas, V.G. Melt Structure and Dynamics of Unentangled Polyethylene Rings: Rouse Theory, Atomistic Molecular Dynamics Simulation, and Comparison with the Linear Analogues. *Macromolecules* **2010**, *43*, 10692–10713, doi:10.1021/ma1017555.
3. Stephanou, P.S.; Mavrantzas, V.G. Accurate Prediction of the Linear Viscoelastic Properties of Highly Entangled Mono and Bidisperse Polymer Melts. *J. Chem. Phys.* **2014**, *140*, 214903, doi:10.1063/1.4878500.
4. Smith, D.E.; Babcock, H.P.; Chu, S. Single-Polymer Dynamics in Steady Shear Flow. *Science (80-.).* **1999**, *283*, 1724–1727, doi:10.1126/science.283.5408.1724.
5. LeDuc, P.; Haber, C.; Bao, G.; Wirtz, D. Dynamics of Individual Flexible Polymers in a Shear Flow. *Nature* **1999**, *399*, 564–566, doi:10.1038/21148.
6. Nafar Sefiddashti, M.H.; Edwards, B.J.; Khomami, B. Individual Chain Dynamics of a Polyethylene Melt Undergoing Steady Shear Flow. *J. Rheol.* **2015**, *59*, 119–153, doi:10.1122/1.4903498.
7. Edwards, C.N.; Nafar Sefiddashti, M.H.; Edwards, B.J.; Khomami, B. In-Plane and out-of-Plane Rotational Motion of Individual Chain Molecules in Steady Shear Flow of Polymer Melts and Solutions. *J. Mol. Graph. Model.* **2018**, *81*, 184–196, doi:10.1016/j.jmgm.2018.03.003.

8. Batchelor, G.K.; Green, J.T. The Determination of the Bulk Stress in a Suspension of Spherical Particles to Order C2. *J. Fluid Mech.* **1972**, *56*, 401–427, doi:10.1017/S0022112072002435.
9. Nafar Sefiddashti, M.H.; Edwards, B.J.; Khomami, B. Steady Shearing Flow of a Moderately Entangled Polyethylene Liquid. *J. Rheol.* **2016**, *60*, 1227–1244, doi:10.1122/1.4963800.
10. Kim, J.M.; Baig, C. Precise Analysis of Polymer Rotational Dynamics. *Sci. Rep.* **2016**, *6*, 19127, doi:10.1038/srep19127.
11. Tsamopoulos, A.J.; Katsarou, A.F.; Tsalikis, D.G.; Mavrantzas, V.G. Shear Rheology of Unentangled and Marginally Entangled Ring Polymer Melts from Large-Scale Nonequilibrium Molecular Dynamics Simulations. *Polymers (Basel).* **2019**, *11*, 1194, doi:10.3390/polym11071194.
12. Schroeder, C.M.; Teixeira, R.E.; Shaqfeh, E.S.G.; Chu, S. Dynamics of DNA in the Flow-Gradient Plane of Steady Shear Flow: Observations and Simulations. *Macromolecules* **2005**, *38*, 1967–1978, doi:10.1021/ma0480796.
13. Schroeder, C.M.; Teixeira, R.E.; Shaqfeh, E.S.G.; Chu, S. Characteristic Periodic Motion of Polymers in Shear Flow. *Phys. Rev. Lett.* **2005**, *95*, 018301, doi:10.1103/PhysRevLett.95.018301.
14. Huang, C.C.; Sutmann, G.; Gompper, G.; Winkler, R.G. Tumbling of Polymers in Semidilute Solution under Shear Flow. *EPL* **2011**, *93*, 54004, doi:10.1209/0295-5075/93/54004.
15. Xu, X.; Chen, J.; An, L. Shear Thinning Behavior of Linear Polymer Melts under Shear Flow via Nonequilibrium Molecular Dynamics. *J. Chem. Phys.* **2014**, *140*, 174902, doi:10.1063/1.4873709.
16. Stephanou, P.S.; Schweizer, T.; Kröger, M. Communication: Appearance of Undershoots in Start-up Shear: Experimental Findings Captured by Tumbling-Snake Dynamics. *J. Chem. Phys.* **2017**, *146*, 161101, doi:10.1063/1.4982228.
17. Costanzo, S.; Huang, Q.; Ianniruberto, G.; Marrucci, G.; Hassager, O.; Vlassopoulos, D. Shear and Extensional Rheology of Polystyrene Melts and Solutions with the Same Number of Entanglements. *Macromolecules* **2016**, *49*, 3925–3935, doi:10.1021/acs.macromol.6b00409.
18. Gordon, R.J.; Schowalter, W.R. Anisotropic Fluid Theory: A Different Approach to the Dumbbell Theory of Dilute Polymer Solutions. *Trans Soc Rheol* **1972**, *16*, 79–97, doi:10.1122/1.549256.
19. Johnson, M.W.; Segalman, D. A Model for Viscoelastic Fluid Behavior Which Allows Non-Affine Deformation. *J. Nonnewton. Fluid Mech.* **1977**, *2*, 255–270, doi:10.1016/0377-0257(77)80003-7.
20. Larson, R.G. *Constitutive Equations for Polymer Melts and Solutions*; 1st ed.; Butterworth-Heinemann, 1988; ISBN 978-0-409-90119-1.
21. Öttinger, H.C. *Beyond Equilibrium Thermodynamics*; John Wiley and Sons, 2005; ISBN 0471666580.
22. Stephanou, P.S.; Baig, C.; Mavrantzas, V.G. A Generalized Differential Constitutive Equation for Polymer Melts Based on Principles of Nonequilibrium Thermodynamics. *J. Rheol.* **2009**, *53*, 309–337, doi:10.1122/1.3059429.
23. Beris, A.N.; Edwards, B.J. *Thermodynamics of Flowing Systems: With Internal Microstructure*; Oxford University Press: New York, 1994; ISBN 019507694X.
24. Stephanou, P.S. The Rheology of Drilling Fluids from a Non-Equilibrium Thermodynamics Perspective. *J. Pet. Sci. Eng.* **2018**, *165*, 1010–1020, doi:10.1016/j.petrol.2017.11.040.
25. Hinch, E.J. Mechanical Models of Dilute Polymer Solutions in Strong Flows. *Phys. Fluids* **1977**, *20*, S22–S30, doi:10.1063/1.861735.
26. Rallison, J.M.; Hinch, E.J. Do We Understand the Physics in the Constitutive Equation? *J. Nonnewton. Fluid Mech.* **1988**, *29*, 37–55, doi:10.1016/0377-0257(88)85049-3.
27. Beris, A.N.; Stiakakis, E.; Vlassopoulos, D. A Thermodynamically Consistent Model for the Thixotropic Behavior of Concentrated Star Polymer Suspensions. *J. Nonnewton. Fluid Mech.* **2008**, *152*, 76–85, doi:10.1016/j.jnnfm.2007.10.016.
28. Stephanou, P.S.; Kröger, M. Non-Constant Link Tension Coefficient in the Tumbling-Snake Model Subjected to Simple Shear. *J. Chem. Phys.* **2017**, *147*, 174903, doi:10.1063/1.4991935.
29. Stephanou, P.S.; Kröger, M. Solution of the Complete Curtiss-Bird Model for Polymeric Liquids Subjected to Simple Shear Flow. *J. Chem. Phys.* **2016**, *144*, 124905, doi:10.1063/1.4944674.
30. Stephanou, P.S.; Kröger, M. From Intermediate Anisotropic to Isotropic Friction at Large Strain Rates to Account for Viscosity Thickening in Polymer Solutions. *J. Chem. Phys.* **2018**, *148*, 184903-undefined, doi:10.1063/1.5019337.
31. Stephanou, P.S.; Georgiou, G.G. A Nonequilibrium Thermodynamics Perspective of Thixotropy. *J. Chem. Phys.* **2018**, *149*, 244902, doi:10.1063/1.5049397.
32. Stephanou, P.S.; Tsimouri, I.C. A Constitutive Hemorheological Model Addressing the Deformability of Red Blood Cells in Ringer Solutions. *Soft Matter* **2020**, *16*, 7585–7597, doi:10.1039/d0sm00974a.
33. Stephanou, P.S. On the Consistent Modeling of Shear-Thickening Polymer Solutions. *Phys. Fluids* **2021**, *33*, 063107, doi:10.1063/5.0053604.
34. Housiadas, K.D.; Beris, A.N. Extensional Behavior Influence on Viscoelastic Turbulent Channel Flow. *J. Nonnewton. Fluid Mech.* **2006**, *140*, 41–56, doi:10.1016/j.jnnfm.2006.03.017.
35. Stephanou, P.S.; Tsimouri, I.C.; Mavrantzas, V.G. Simple, Accurate and User-Friendly Differential Constitutive Model for the Rheology of Entangled Polymer Melts and Solutions from Nonequilibrium Thermodynamics. *Materials (Basel).* **2020**, *13*, 2867, doi:10.3390/ma13122867.
36. Souvaliotis, A.; Beris, A.N. An Extended White–Metzner Viscoelastic Fluid Model Based on an Internal Structural Parameter. *J. Rheol.* **1992**, *36*, 241–271, doi:10.1122/1.550344.
37. Siepmann, J.I.; Karaborni, S.; Smit, B. Simulating the Critical Behaviour of Complex Fluids. *Nature* **1993**, *365*, 330–332, doi:10.1038/365330a0.

38. Plimpton, S. Fast Parallel Algorithms for Short-Range Molecular Dynamics. *J. Comput. Phys.* **1995**, *117*, 1–19, doi:10.1006/jcph.1995.1039.
39. Nosé, S. Constant Temperature Molecular Dynamics Methods. *Prog. Theor. Phys. Suppl.* **1991**, *103*, 1–46, doi:10.1143/ptps.103.1.
40. Parrinello, M.; Rahman, A. Polymorphic Transitions in Single Crystals: A New Molecular Dynamics Method. *J. Appl. Phys.* **1981**, *52*, 7182–7190, doi:10.1063/1.328693.
41. Todd, B.D.; Daivis, P.J. *Nonequilibrium Molecular Dynamics: Theory, Algorithms and Applications*; Cambridge University Press: Cambridge, U.K., 2017;
42. Tuckerman, M.; Berne, B.J.; Martyna, G.J. Reversible Multiple Time Scale Molecular Dynamics. *J. Chem. Phys.* **1992**, *97*, 1990–2001, doi:10.1063/1.463137.
43. Williams, G.; Watts, D.C. Non-Symmetrical Dielectric Relaxation Behaviour Arising from a Simple Empirical Decay Function. *Trans. Faraday Soc.* **1970**, *66*, 80–85, doi:10.1039/TF9706600080.
44. MathWorks, T. MATLAB (R2020b). *MathWorks Inc.* 2020.
45. Grmela, M. Stress Tensor in Generalized Hydrodynamics. *Phys. Lett. A* **1985**, *111*, 41–44, doi:10.1016/0375-9601(85)90798-4.